Rare Metal Materials and Engineering
Volume 55, Issue 9, September 2026
Available online at www.rmme.ac.cn

Science Press

Cite this article as: Zhou Yongkang, Zhao Ziyan, Wang Yuanyuan, et al. Effect of Zr/Ta Ratio on Microstructure and Mechanical Properties of Zr-Ti-Nb-Ta Refractory High-Entropy Alloys[J]. Rare Metal Materials and Engineering, 2026, 55(09): 2142-2148. DOI: https://doi.org/10.12442/j.issn.1002-185X.20250513.

ARTICLE

Effect of Zr/Ta Ratio on Microstructure and Mechanical Properties of Zr-Ti-Nb-Ta Refractory High-Entropy Alloys

Zhou Yongkang, Zhao Ziyan, Wang Yuanyuan, Yin Kexin, Li Hong, Li Zhengkun, Zhang Haifeng, Zhu Zhengwang

Research Center of Advanced Metastable Metallic Materials, School of Metallurgy, Northeastern University, Shenyang 110819, China

Abstract: Optimal combination of strength and ductility for refractory high-entropy alloys (RHEAs) can be achieved by regulating the alloy composition that induces the mismatch between atomic size and modulus. Thus, the influence of Zr and Ta on the microstructure evolution and room-temperature mechanical properties of $Zr_{45-x}Ti_{15}Nb_{30}Ta_{10+x}$ (x=0, 5, and 10, at %) RHEAs was investigated. Results show that the variation in the Zr/Ta ratio does not change the phase composition of the alloys. All three alloys are only composed of body-centered cubic phase. However, with the decrease in Zr/Ta ratio, the yield strength and ductility of the alloys are increased simultaneously: the yield strength increases from 901 MPa to 1003 MPa, and the elongation increases from 13.3% to 16.1%. The enhancement in ductility is primarily caused by grain refinement and the decrease in lattice distortion. Meanwhile, the increase in yield strength is mainly attributed to the synergistic effect of the increased shear modulus mismatch induced by the higher Ta content and the grain refinement strengthening. This study provides valuable insights into the influence of composition variation on the properties of RHEAs.

Key words: RHEA; modulus mismatch; atomic size mismatch; microstructure evolution; mechanical property

1 Introduction

Refractory high-entropy alloys (RHEAs), primarily composed of high-melting-point elements, such as Zr, Ti, Nb, Hf, Ta, Mo, and W, have emerged as a pioneering class of materials with exceptional potential for high-temperature applications[1–3]. Because RHEAs usually contain body-centered cubic (bcc)-related elements, they typically exhibit a single bcc structure[4–7]. Owing to their superior high-temperature strength, remarkable resistance against softening, and excellent creep resistance at temperatures exceeding 1000 °C[8–12], RHEAs are considered as promising candidates to replace conventional Ni-based superalloys in critical sectors, such as aerospace, nuclear reactors, and advanced propulsion systems.

Despite their impressive strength retention at elevated temperatures, the industrial application of many pioneering RHEAs, such as NbMoTaW[13], is significantly restricted by their inherent shortcomings. The primary concern is their inadequate room-temperature ductility and inferior fracture toughness, which usually complicate manufacturing processes, such as machining and forging. The HfNbTiZrTa alloys, as the pioneering RHEA system exhibiting extensive tensile ductility, have already paved the way for the development of RHEAs with excellent room-temperature plasticity[14–16]. HfNbTiZrTa alloys can also retain excellent tensile properties at cryogenic temperatures. As the temperature decreases from 277 K to 77 K, the alloy can maintain a high tensile elongation of 20.8%, while its yield strength significantly increases to 1549 MPa with no obvious ductile-to-brittle transition[15]. The Zr-Ti-Nb-Ta system, a variant of the HfNbTiZrTa RHEAs, similarly exhibits excellent tensile properties. Nguyen et al[17] developed a new non-equiatomic $Ti_{40}Zr_{25}Nb_{25}Ta_{10}$ RHEA by controlling the Ti/Ta ratio via the atomic misfit method, demonstrating high tensile strain (>18%) and high strength (>900 MPa) at the as-

Received date: September 30, 2025
Foundation item: Natural Science Foundation of Liaoning Province (2025-BS-0127); Supported by Rare Earth Advanced Materials Technology Innovation Center (CXZX-B-202311-0011); Postdoctoral Science Foundation of Northeastern University (2025-9Y-37)
Corresponding author: Zhu Zhengwang, Ph. D., Professor, Research Center of Advanced Metastable Metallic Materials, School of Metallurgy, Northeastern University, Shenyang 110819, P. R. China, E-mail: zhuzw@mail.neu.edu.cn

cast condition. Moreover, this non-equiatomic design strategy avoids introduction of new elements into the single-phase solid-solution RHEA, thereby preventing or at least minimizing the formation of unintended intermetallic compounds.

Solid solution strengthening, synergistically governed by atomic size mismatch and modulus mismatch, is widely recognized as a key reason for the high strength of RHEAs[14]. Among elements Ti, Zr, Nb, and Ta, element Zr possesses the largest atomic size (r_{Ti}=141.9 pm; r_{Zr} = 154.3 pm; r_{Nb} = 142.9 pm; r_{Ta}=143.0 pm)[18]. Increasing the Zr content can enhance the atomic size mismatch, thereby inducing severe lattice distortion and improving the alloy strength. Based on this theory, Zr-rich RHEAs, such as $Zr_{45}Ti_{15}Nb_{30}Ta_{10}$ and $Zr_{45}Ti_{15}Nb_{20}Ta_{20}$, were designed[19–21]. Results showed that the tensile strain exceeded 13% at room temperature, and the tensile strength reached 1150 MPa[19–21]. As Ta possesses the highest shear modulus in this system (G_{Ta}=69 GPa; G_{Zr}=22 GPa; G_{Ti}=27 GPa; G_{Nb}=37 GPa), the shear modulus mismatch exhibits a positive correlation with the Ta content. The Zr/Ta ratio effectively plays a significant role in atomic size mismatch and shear modulus mismatch, thus governing the structure and properties of alloys.

In this research, based on the previously designed $Zr_{45}Ti_{15}Nb_{30}Ta_{10}$ RHEA[21], the Zr/Ta ratio was modulated, and the new non-equiatomic $Zr_{40}Ti_{15}Nb_{30}Ta_{15}$ and $Zr_{35}Ti_{15}Nb_{30}Ta_{20}$ RHEAs were developed. The influence of the Zr/Ta ratio on the microstructure and mechanical properties was investigated. The findings showed that decreasing the Zr/Ta ratio significantly refined the alloy grains and simultaneously improved the strength and plasticity.

2 Experiment

Three non-equiatomic $Zr_{45}Ti_{15}Nb_{30}Ta_{10}$, $Zr_{40}Ti_{15}Nb_{30}Ta_{15}$, and $Zr_{35}Ti_{15}Nb_{30}Ta_{20}$ RHEAs were fabricated with high-purity metal nuggets of Zr, Ti, Nb, and Ta (>99.95wt%) by arc melting and denoted as Zr45-Ta10, Zr40-Ta15, and Zr35-Ta20 samples, respectively. The Zr-Ti and Nb-Ta master alloys were firstly prepared separately to ensure the homogeneous melting, and then they were melted together and solidified into button ingots. Under the protection of high-purity argon gas, the button ingots were remelted, mixed thoroughly, and remelted at least 7 times to ensure chemical homogeneity. Subsequently, the samples were cast into a water-cooled copper mold (8 mm×12 mm× 40 mm).

The crystal structure of RHEAs was characterized using an X-ray diffractometer (XRD, Rigaku D/max-2500PC) with Cu Kα radiation operated at 40 kV/40 mA. The scanning was performed over a 2θ range from 20° to 100° at a scan rate of 10°/min. The microstructure was characterized using a field-emission scanning electron microscope (SEM, Zeiss Sigma 300) equipped with an electron backscatter diffractometer (EBSD, Zeiss C-Nano) and an energy-dispersive spectroscope (EDS) system. For EBSD analysis, the samples were electro-chemically polished at −30 °C in an electrolyte consisting of 10vol% perchloric acid and 90vol% methanol, using a voltage of 25 V for 25 s. The dislocation structure was characterized using a transmission electron microscope (TEM, FEI Talos F200X G2) operated at an accelerating voltage of 200 kV. TEM samples with diameter of 3 mm were mechanically ground to the ones with thickness of 30 μm. Then, they were ion-milled until perforation using a Gatan 695 device.

Dog-bone-shaped tensile samples with rectangular cross-sections (15 mm×2 mm×1 mm) were machined and polished under the as-cast condition. Quasi-static uniaxial tensile tests were conducted on a universal testing machine (Instron-5582, Instron, USA) with an initial strain rate of 1×10^{-3} s^{-1}. To ensure the reliability of the data, tensile tests were performed 3 times under each condition.

3 Results and Discussion

3.1 Microstructure of Zr-Ti-Nb-Ta RHEAs

The phase constituents of the as-cast RHEAs were characterized by XRD, as presented in Fig. 1. The results indicate that the variations in Zr/Ta ratio do not alter the phase composition of the alloys, and all three samples exhibit single bcc structure. The thermodynamic parameters of the samples are listed in Table 1, which all fall within the range conducive to the formation of the bcc phase. Based on the position of (110) diffraction peak, a gradual shift toward higher 2θ value can be observed with the decrease in Zr/Ta ratio (i.e., with the increase in Ta content), and the 2θ value increases from 36.934°

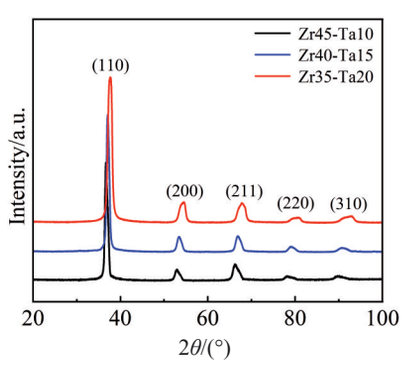

Fig.1 XRD patterns of as-cast Zr45-Ta10, Zr40-Ta15, and Zr35-Ta20 RHEAs

Table 1 Thermodynamic parameters of Zr45-Ta10, Zr40-Ta15, and Zr35-Ta20 RHEAs

RHEA	Mixing enthalpy, ΔH_{mix}/kJ·mol^{-1}	Mixing entropy, ΔS_{mix}/J·(K·mol)$^{-1}$	Atomic size mismatch, δ/%	Ω	Valence electron concentration, VEC
Zr45-Ta10	3.12	10.27	6.30	7.14	4.40
Zr40-Ta15	3.09	10.93	6.28	8.71	4.45
Zr35-Ta20	3.00	11.10	6.17	9.32	4.50

to 37.835°, which indicates a corresponding decrease in lattice parameter. This lattice contraction can be primarily attributed to the smaller atomic radius of Ta, compared with that of Zr.

The microstructure of the as-cast RHEAs was characterized by EBSD analysis, as shown in Fig. 2a–2c. The inverse pole figures (IPFs) reveal that no preferred orientation can be observed in any as-cast RHEAs. The grain size decreases from 27 μm (Zr45-Ta10) to 17 μm (Zr35-Ta20). The reduction in grain size is primarily attributed to the variation in chemical composition, i. e., a decrease in the Zr/Ta ratio and a concomitant increase in Ta content. The higher melting point of Ta, compared with that of Zr, increases the undercooling at the solid-liquid interface during solidification[22]. Meanwhile, the increase in Ta increases the melting point of the alloy system, thereby raising the activation energy required for recrystallization and suppressing grain growth. Therefore, a decrease in Zr/Ta ratio causes a decrease in grain size.

3.2 Mechanical properties of Zr-Ti-Nb-Ta RHEAs

The mechanical properties of the Zr45-Ta10, Zr40-Ta15, and Zr35-Ta20 RHEAs were characterized by room-temperature tensile tests, and the results are shown in Fig. 3. The yield strength (σ_{YS}) and fracture elongation are 901±7 MPa and 13.3%±0.3% for Zr45-Ta10 RHEA, respectively; σ_{YS} and fracture elongation are 979±8 MPa and 14.0%±0.5% for Zr40-Ta15 RHEA, respectively; σ_{YS} and fracture elongation are 1003±10 MPa and 16.1%±0.8% for Zr35-Ta20 RHEA, respectively. The strength and ductility of the alloys are increased simultaneously with the decrease in Zr/Ta ratio.

Solid solution strengthening is one of the primary contributors to the excellent mechanical properties of RHEAs. It originates mainly from the elastic interaction between moving dislocations and local elastic stress fields induced by inherent lattice distortion[14,23]. The severe lattice distortion originates from the interactions among solute atoms due to the mismatches in shear modulus and atomic radius. The atomic radius mismatch δr_{ij} and shear modulus mismatch δu_{ij} between different atom pairs can be expressed by Eq.(1–2)[22], respectively:

$$\delta r_{ij} = \left| 2(r_i - r_j)/(r_i + r_j) \right| \quad (1)$$

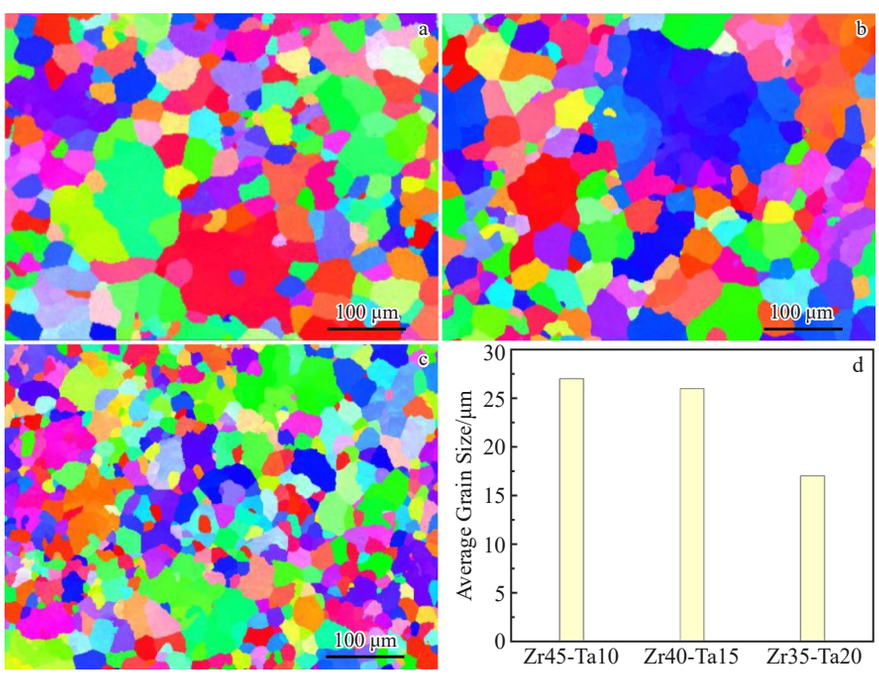

Fig.2 IPFs of Zr45-Ta10 (a), Zr40-Ta15 (b), and Zr35-Ta20 (c) RHEAs; average grain sizes of different RHEAs (d)

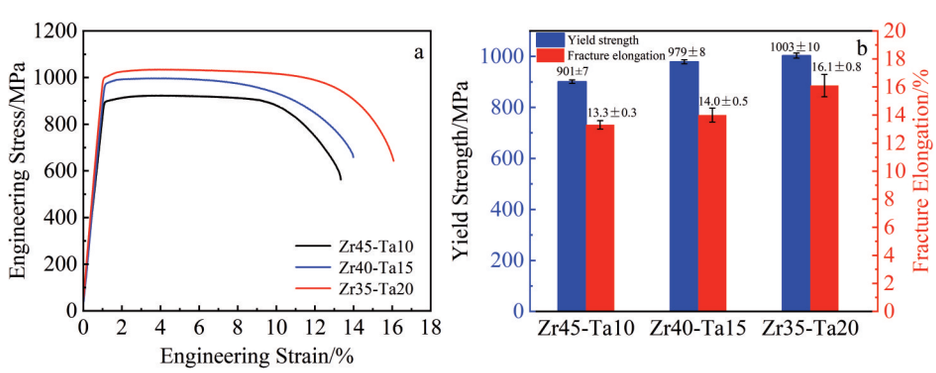

Fig.3 Engineering stress-engineering strain curves (a) and yield strength with fracture elongation (b) of as-cast Zr45-Ta10, Zr40-Ta15, and Zr35-Ta20 RHEAs

$$\delta u_{ij} = \left| 2(u_i - u_j)/(u_i + u_j) \right| \quad (2)$$

where r_i and u_i represent the atomic radius and shear modulus of element i, respectively; r_j and u_j represent the atomic radius and shear modulus of element j, respectively. Table 2 presents the calculated results. The average values of shear modulus mismatch (δ_u^{ave}) and atomic radius mismatch (δ_r^{ave}) in RHEAs can be expressed by Eq.(3–4), respectively:

$$\delta_r^{ave} = (c_1, c_2, \cdots, c_n) \begin{pmatrix} 0 & \delta r_{12} & \cdots & \delta r_{1n} \\ \delta r_{21} & \ddots & \vdots & \delta r_{2n} \\ \vdots & \cdots & 0 & \vdots \\ \delta r_{n1} & \delta r_{n2} & \cdots & 0 \end{pmatrix} \begin{pmatrix} c_1 \\ c_2 \\ \vdots \\ c_n \end{pmatrix} \quad (3)$$

$$\delta_u^{ave} = (c_1, c_2, \cdots, c_n) \begin{pmatrix} 0 & \delta u_{12} & \cdots & \delta u_{1n} \\ \delta u_{21} & \ddots & \vdots & \delta u_{2n} \\ \vdots & \cdots & 0 & \vdots \\ \delta u_{n1} & \delta u_{n2} & \cdots & 0 \end{pmatrix} \begin{pmatrix} c_1 \\ c_2 \\ \vdots \\ c_n \end{pmatrix} \quad (4)$$

where c_1, c_2, $\cdots$, c_n present the atomic percentage of the elements i (i=1–n). Therefore, the δ_u^{ave} and δ_r^{ave} values are 0.039 and 0.299 for Zr45-Ta10 RHEA, respectively; the δ_u^{ave} and δ_r^{ave} values are 0.036 and 0.337 for Zr35-Ta20 RHEA, respectively. As the Zr/Ta ratio decreases, the δ_r^{ave} exhibits a slight reduction from 0.039 to 0.036, whereas the δ_u^{ave} shows a significant increase from 0.299 to 0.337. Therefore, the enhancement in strength is primarily attributed to solid solution strengthening resulting from the increase in average shear modulus[22].

Additionally, grain refinement typically leads to a strengthening effect, which can be quantified using the Hall-Petch relationship[24], as follows:

$$\sigma_y = \sigma_0 + kd^{-1/2} \quad (5)$$

where σ_y is yield strength, d is average grain size, σ_0 is a constant regarded as the frictional stress or internal back stress caused by dislocation motion, and k is a constant considered to measure the resistance of grain boundaries against slip (430 MPa·μm$^{1/2}$)[25]. Since the grain sizes differ slightly, the grain refinement contributes to an increment of only 22 MPa to the yield strength.

The improvement in ductility can be partially attributed to the reduced lattice distortion, which decreases from 6.30% to 6.17%, thereby weakening the local stress fields. Besides, the fine-grained microstructure of the Zr15-Ti45 alloy results in a larger number of grains per unit volume, enabling the plastic deformation to be more homogeneously distributed and accommodated by a greater number of grains. As a result, dislocation pile-ups within individual grains are reduced, thereby decreasing the likelihood of crack initiation caused by stress concentration and enabling the material to sustain greater plastic deformation before fracture. Furthermore, finer grains lead to a larger total grain boundary area and more tortuous boundaries, which can more effectively inhibit the crack propagation. Consequently, the Zr35-Ta20 RHEA exhibits enhanced tensile ductility.

Obviously, the Zr35-Ta20 RHEA in this research exhibits a superior combination of strength and elongation under room-temperature tensile deformation, compared with other alloys in Zr-Ti-Nb-Ta RHEA system, as shown in Fig. 4[15,17,20–21,26–30]. In the Zr35-Ta20 RHEA, Ta exhibits smaller atomic dimensions and the highest shear modulus. Consequently, reducing the Zr/Ta ratio correspondingly decreases lattice distortion, which contributes to the enhanced plasticity of the alloy. Besides, Ta also alters the local shear stress distribution, promoting the formation of twist bands and improving the

Table 2 Atomic radius mismatch δr_{ij} and shear modulus mismatch $\delta \mu_{ij}$ for different atom pairs

δr_{ij} \ $\delta \mu_{ij}$		Element *i*			
		Zr	Ti	Nb	Ta
Element *j*	Zr	0	0.084	0.077	0.076
	Ti	0.204	0	0.007	0.008
	Nb	0.533	0.338	0	0.001
	Ta	1.033	0.875	0.579	0

coordination of slip systems. Furthermore, Ta simultaneously increases shear modulus mismatch, thereby enhancing the strength of the alloy through solid solution strengthening.

To elucidate the deformation mechanisms of RHEA, the deformed microstructure of the tensile fracture was characterized, as shown in Fig. 5. Compared with the mixed morphology of dimples and cleavage planes in the Zr45-Ta10 RHEA (Fig. 5a–5b), the presence of fine and deep dimples on the fracture surface of the Zr35-Ta20 RHEA (Fig. 5c – 5d) indicates its capability to undergo substantial plastic elongation before failure. EBSD analysis near the fracture surface indicates that the Zr35-Ta20 RHEA exhibits a uniform distribution of internal strain, while in the Zr45-Ta10 RHEA[21], the strain is predominantly accumulated near the

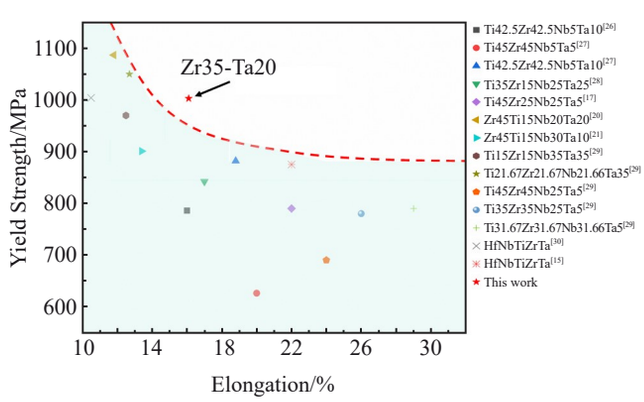

Fig.4 Comparison of mechanical properties of representative Zr-Ti-Nb-Ta RHEAs[15,17,20–21,26–30]

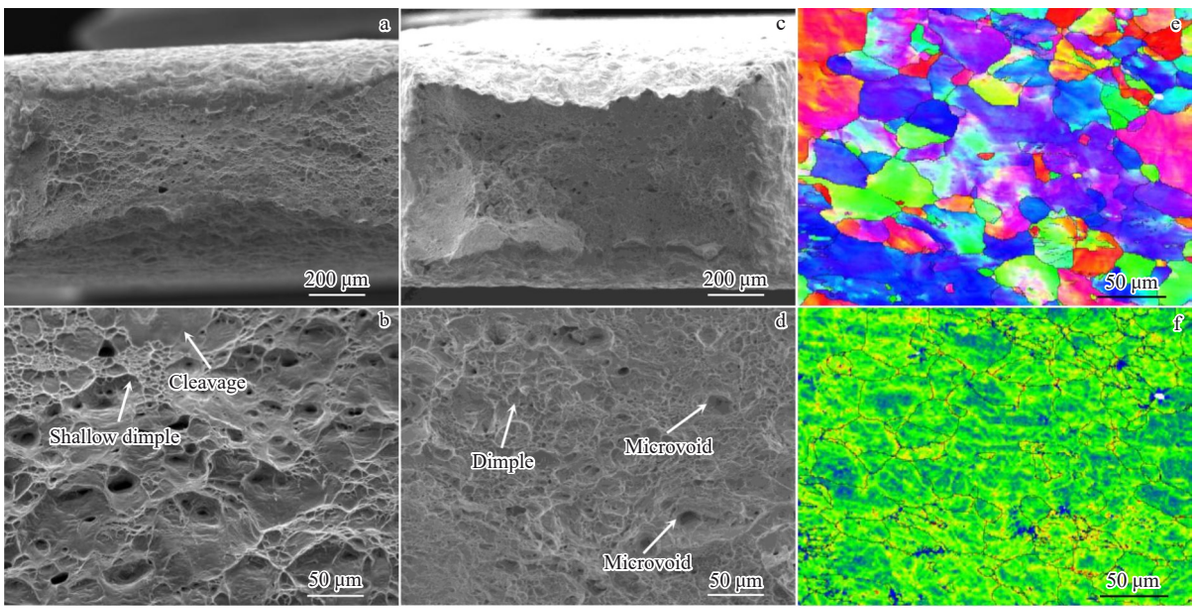

Fig.5 Tensile fracture morphologies of Zr45-Ta10 (a–b) and Zr35-Ta20 (c–d) RHEAs; EBSD images of deformation structure near the fracture area of Zr35-Ta20 RHEA (e–f)

grain boundaries with an inhomogeneous distribution, including some strain-free grains. This observation is consistent with the superior tensile ductility of Zr35-Ta20 RHEA.

Subsequently, the deformation microstructure near the fracture surface of the Zr35-Ta20 alloy was observed using TEM, as shown in Fig. 6. Fig. 6a shows planar dislocation arrays resulting from the planar slip, which are typically aligned along the tensile axis. Fig. 6b shows slip bands with a width of 100 nm, within which the dislocations of high density are distributed, as indicated by the white dotted lines. Furthermore, dislocation fragmentation structures resulting from cross-slip can be observed, which provide compelling evidence that the primary deformation mode of the alloy is dominated by cross-slip[31]. Fig. 6c – 6d reveal that the dislocations are obstructed and accumulated at the grain boundaries, resulting in mutual entanglement. Grain boundaries act as not only dislocation sources but also barriers to dislocation motion[32–34]. When the dislocations glide to grain boundaries, their movement is hindered, prompting the

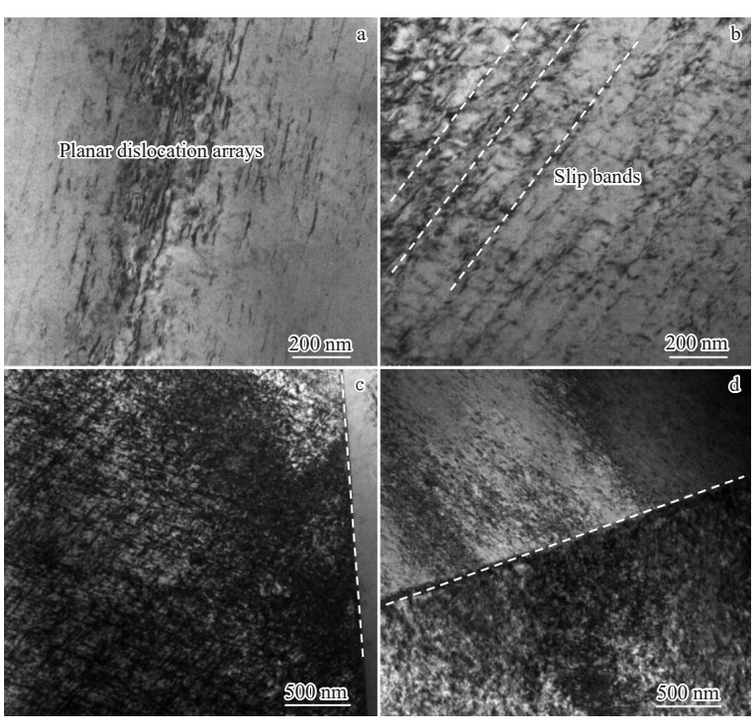

Fig.6 TEM bright field images of Zr35-Ta20 RHEA after fracture

generation of numerous dislocations in the vicinity. Therefore, increasing the grain boundary density of the alloy promotes more uniform dislocation distribution, as shown in Fig. 6c, thereby enhancing the capacity of the alloy for homogeneous deformation. Meanwhile, Fig.6c reveals a coplanar dislocation array. Such coplanar slip facilitates dislocation nucleation and multiplication, homogenizes the dislocation substructure, and delays the onset of necking, thereby enhancing the overall ductility. This is further evidenced by the elongated ductile dimples observed on the fracture surface.

4 Conclusions

1) The Zr/Ta ratio does not alter the phase structure of the Zr45-Ta10, Zr40-Ta15, and Zr35-Ta20 RHEAs: they all consist of single bcc phase. As the Zr/Ta ratio decreases, the grain size decreases from 27 μm to 17 μm.

2) $Zr_{45-x}Ti_{15}Nb_{30}Ta_{10+x}$ RHEAs exhibit simultaneous increase in strength and ductility as the Zr/Ta ratio decreases. Among them, the Zr35-Ta20 RHEA displays optimal mechanical properties with the yield strength of 1003 MPa and fracture elongation of 16.1%.

3) The enhancement in strength for the Zr35-Ta20 RHEA results from the synergistic effect of solid solution strengthening induced by shear modulus mismatch and grain refinement strengthening. The improvement in plasticity is primarily attributed to the reduction in atomic size mismatch, which leads to a decrease in the local stress field.

References

1 George E P, Raabe D, Ritchie R O. *Nature Reviews Materials*[J], 2019, 4(8): 515

2 Senkov O N, Senkova S V, Woodward C *et al*. *Acta Materialia*[J], 2013, 61(5): 1545

3 Wyatt B C, Yang Y, Michałowski P P *et al*. *Science*[J], 2025, 389(6764): 1054

4 Senkov O N, Semiatin S L. *Journal of Alloys and Compounds*[J], 2015, 649: 1110

5 Couzinié J P, Lilensten L, Champion Y *et al*. *Materials Science and Engineering A*[J], 2015, 645: 255

6 Zou Y, Maiti S, Steurer W *et al*. *Acta Materialia*[J], 2014, 65: 85

7 Li T, Jiao W, Miao J *et al*. *Materials Science and Engineering A*[J], 2021, 827: 142061

8 Maresca F, Curtin W A. *Acta Materialia*[J], 2020, 182: 235

9 Senkov O N, Wilks G B, Miracle D B *et al*. *Intermetallics*[J], 2010, 18(9): 1758

10 Zhou Y K, Zeng S, Zhu Y H *et al*. *Metallurgical and Materials Transactions A*[J], 2022, 53(10): 3669

11 Sahragard M G, Belcher C H, Bajpai S *et al*. *Acta Materialia*[J], 2024, 272: 119940

12 Li T X, Lu Y P, Li Z Q *et al*. *Intermetallics*[J], 2022, 146: 107586

13 Senkov O N, Wilks G B, Scott J M *et al*. *Intermetallics*[J], 2011, 19(5): 698

14 Senkov O N, Scott J M, Senkova S V *et al*. *Journal of Alloys and Compounds*[J], 2011, 509(20): 6043

15 Wang S B, Wu M X, Shu D *et al*. *Acta Materialia*[J], 2020, 201: 517

16 Mills L H, Emigh M G, Frey C H *et al*. *Acta Materialia*[J], 2023, 245: 118618

17 Nguyen V T, Qian M, Shi Z *et al*. *Materials Science and Engineering A*[J], 2019, 742: 762

18 Nguyen V T, Qian M, Shi Z. *et al Intermetallics*[J], 2018, 101: 39

19 Zhou Y K, Zeng S, Zhang H W *et al*. *Journal of Materials Science & Technology*[J], 2024, 187: 101

20 Zhou Y K, Zeng S, Zhu Y H *et al*. *Materials Letters*[J], 2022, 324: 132779

21 Zhou Y K, Zeng S, Li H *et al*. *Materials Science and Engineering A*[J], 2023, 874: 145091

22 Zhou Y K, Liu X Y, Chen J Q *et al*. *Materials Science and Engineering A*[J], 2025, 923: 147696

23 Wang H, Yang P Y, Zhao W J *et al*. *Nature Communications*[J], 2024, 15(1): 6782

24 Hansen N. *Scripta Materialia*[J], 2004, 51(8): 801

25 Coury F G, Kaufman M, Clarke A J. *Acta Materialia*[J], 2019, 175: 66

26 Li Z, Lai W J, Wang B B *et al*. *Intermetallics*[J], 2022, 151: 107731

27 Li Z, Lai W J, Tong X *et al Materials Science and Engineering A*[J], 2022, 845: 143203

28 Mustafi L, Nguyen V T, Lu S L *et al*. *Materials Science and Engineering A*[J], 2021, 824: 141805

29 Yuan Y, Wu Y F, Yang Z L *et al*. *Materials Research Letters*[J], 2019, 7(6): 225

30 Xu L, Jia Y F, Ma Y L *et al*. *Journal of Materials Science & Technology*[J], 2025, 209: 240

31 Li T L, Wang S D, Fan W X *et al*. *Acta Materialia*[J], 2023, 246: 118728

32 Cheng S, Spencer J A, Milligan W W. *Acta Materialia*[J], 2003, 51(15): 4505

33 Horita Z, Smith D J, Furukawa M *et al*. *Journal of Materials Research*[J], 1996, 11(8): 1880

34 Zeng H L, Han M Y Q, Li B L *et al*. *Microstructures*[J], 2025, 5(1): 2025010

Zr/Ta比对Zr-Ti-Nb-Ta难熔高熵合金微观组织及力学性能的影响

周永康，赵子彦，王媛媛，尹可心，李　宏，李正坤，张海峰，朱正旺
(东北大学 冶金学院 先进亚稳金属材料研究中心，辽宁 沈阳 110819)

摘　要：通过调控诱发原子尺寸与模量错配的合金组元，实现难熔高熵合金强度与延展性的最优组合，研究了Zr和Ta对$Zr_{45-x}Ti_{15}Nb_{30}Ta_{10+x}$（$x$=0, 5, 10, at%）难熔高熵合金微观结构演变及室温力学性能的影响。结果表明：Zr/Ta比的变化未改变合金的相结构，3种合金的相组成均为单一的体心立方结构。但随着Zr/Ta比降低，合金的屈服强度与延展性同时提高，屈服强度从901 MPa增加至1003 MPa，延展性从13.3%提高至16.1%。延展性提升主要源于晶粒细化与晶格畸变减小；而强度增长则主要归因于高Ta含量引发的剪切模量失配增强与细晶强化之间的协同作用。本研究为成分变化对难熔高熵合金性能的影响提供了重要认识。

关键词：难熔高熵合金；模量错配；原子尺寸错配；微观结构演变；力学性能

作者简介：周永康，男，1994年生，博士，东北大学冶金学院先进亚稳金属材料研究中心，辽宁 沈阳 110819，E-mail：zhouyk@smm.neu.edu.cn